https://doi.org/10.20965/jrm.2013.p0252

Paper:

Characterization of Deformable Objects by Using Dynamic Nonprehensile Manipulation

Ixchel G. Ramirez-Alpizar, Mitsuru Higashimori, and Makoto Kaneko

Graduate School of Engineering, Osaka University
2-1 Yamadaoka, Suita, Osaka 565-0871, Japan
E-mail: {ixchel@hh., higashi@, mk@}mech.eng.osaka-u.ac.jp

[Received October 23, 2012; accepted November 30, 2012]

This paper presents a method for evaluating a physical parameter of unknown deformable objects, by using nonprehensile manipulation. By means of simulation analysis, we show that the curve representing the relationship between the object's angular velocity and the plate's frequency has a resonance-like response. Based on the above phenomenon, we utilize a Lorentz curve fitting to represent the object's angular velocity as a function of the plate's frequency with a simple mathematical expression, instead of deriving the equation of motion of the system that is rather complex due to the intricate dynamics of the system. Then, we show that the first order natural angular frequency in bending determines the frequency at which the object's has its maximal angular velocity. Using this information, we present a method of how to estimate the object's first order natural frequency in bending. We show the simulation and experimental results to verify the validity of the method presented.

Keywords: deformable object, dynamic skill, nonprehensile manipulation, resonant behavior

1. Introduction

In general, robotic manipulation can be classified into two main branches: grasping manipulation and nonprehensile manipulation. The former makes use of fingers to grasp or pick the object with dexterity and precision; while the latter uses a plate or a probe and manipulates the object without grasping it, compensating the dexterity and precision of the former with high speed and simple movements [1–10]. We have already developed a dynamic nonprehensile manipulation scheme inspired by the handling of the pizza peel and made clear how to control the position and orientation of a rigid object on a plate [11]. This manipulation scheme has the advantage that it can remotely manipulate objects by using a simple flat plate with the assistance of vision, therefore allowing the robot to operate the object in areas with high temperatures, high humidity, electromagnetic fields, etc, where electrical hardware is unavailable or where humans can be in danger. Applying this manipulation scheme to handle a deformable object, it also has the advantage of reducing the concentration of stress on the object, thus avoiding the object's destruction. Based on this consideration, we have tried to control the posture of a deformable object on a plate [12], as shown in **Fig. 1(a)**. Through a basic experiment and simulation analysis, we have found that a deformable object changes its angular velocity with an analogy to bipedal gaits [13]. We also found that the object's angular velocity can be represented with a simple mathematical expression [14]. Here, we would like to point out an interesting observation. In this manipulation scheme, the object's high frequency in bending vibration of 10 Hz order shown in **Fig. 1(b)** is converted to a low frequency rotating motion of $f_B \approx 1$ Hz order, as illustrated in **Fig. 1(a)**, due to the object's bipedal gait-like behavior.[1] This suggests that the information of the natural bending frequency of $f_n \approx 10$ Hz order when using comestible products such as cheese or ham, is included in the frequency of rotation of the object, that is, the object's angular velocity. Therefore, we may be able to estimate f_n by only observing the object's low rotation frequency, as an inverse problem. An important advantage is that as we only have to deal with the object's low rotation frequency, a normal camera with 30 fps can be utilized. Otherwise, to directly observe the object's high bending vibration frequency, a high-speed camera with hundreds or thousands fps order is required to guarantee a high accuracy in the measurements. This kind of nonprehensile

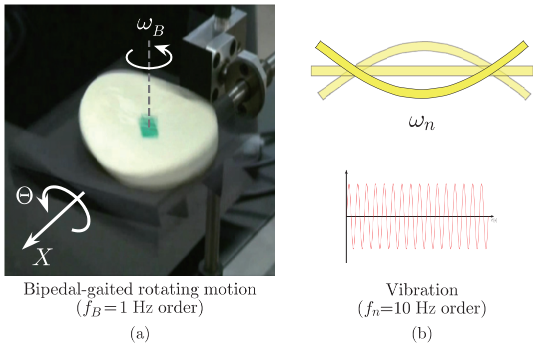

Fig. 1. The low angular velocity of the object ω_B in (a) and the object's high natural angular frequency in bending ω_n (b).

1. If the object is divided into two equal parts and each of them is regarded as left leg and right leg, the rotational motion of the object is similar to a biped gait on the floor. See details in [13].

approach for sensing the parameters of an object may be applicable to the evaluation of freshness and texture of food, which alters the bending frequency of food. Additionally, as this manipulation scheme can prevent a large concentration of stress, it is also expected to significantly contribute to the cell/tissue processing technology in the bioscience research. A change in tissue stiffness could be an indicator of some diseases such as cancer. In our approach the bending frequency may be used as a stiffness evaluation index.

Extending our previous work [14], this paper discusses how to identify the natural bending frequency of deformable objects and shows the simulation and experimental results validating the proposed method. We first show that a thin deformable object can rotate on a vibrating plate with two degrees of freedom, as shown in **Fig. 1(a)**. Next, we show that a deformable object achieves its maximal angular velocity by an appropriate combination of the plate's angular amplitude and frequency, with respect to its physical parameters. Then, we show that the curve describing the relationship between the plate's angular frequency and the object's angular velocity has a resonance-like curve. Taking advantage of this similarity, we employ a Lorentzian curve fitting to represent the dynamic characteristics of the object with a simple mathematical expression, instead of the equation of motion that is rather complex and difficult to obtain because of the intricate dynamics of the system. Through simulation analysis, we reveal that the first order natural angular frequency in bending of the object ω_n as shown in **Fig. 1(b)**, strongly dominate one of the Lorentzian curve characteristics. Based on such nature, we propose an identification method to estimate the natural frequency in bending of unknown objects. Finally, we show the simulation and experimental results of estimating the object's frequency for confirming the validity of the proposed method.

This paper is organized as follows: in Section 2, we briefly review related works. In Section 3, we explain the manipulation scheme and the simulation model. In Section 4, we show the curve fitting employed to characterize the transition of the object's angular velocity. In Section 5, we propose an identification method to estimate the natural bending frequency of an object. In Section 6, we show the simulation and experimental results. In Section 7, we give the conclusion of this work.

2. Related Works

There have been various works discussing nonprehensile manipulation. Lynch and Mason have discussed controllability, motion planning, and implementation of planar dynamic nonprehensile manipulation [1]. Amagai and Takase have shown the experiments where an object is manipulated on a plate attached at the tip of a six DOFs manipulator based on visual information [2]. Reznik et al. have developed the Universal Planar Manipulator (UPM) based on a single horizontally-vibrating plate with three DOFs [3], and Reznik and Canny have demonstrated that multiple objects were simultaneously moved toward target directions [4]. Böhringer et al. have developed a model for the mechanics of microactuators together with a sensorless parallel manipulation theory [5] and have discussed algorithms for sensorless positioning and orienting of planar parts using different vibration patterns [6]. They also proposed microassembly of parts using ultrasonic vibration and electrostatic forces to position and align parts in parallel on a vibratory table [7]. Vose et al. have discussed sensorless control methods for point parts sliding on a rigid plate [8]. They have shown that translation and rotation of a rigid plate induces parts on the plate to move toward or away from a nodal line aligned with the rotation axis [9], and how to find frictional velocity fields generated by plate motions [10]. These works done on manipulation utilizing a plate have supposed that the object is a particle(s) or a rigid body(ies). In contrast, prevalent works treating deformable objects generally make use of grasp manipulation [15–18]. The authors have already discussed how to manipulate a deformable object [12, 13].

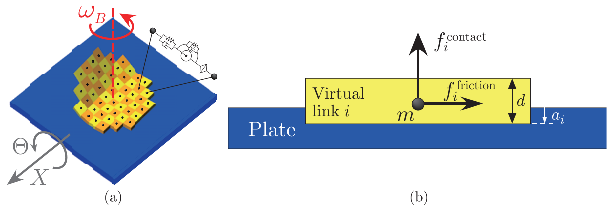

Fig. 2. Dynamic nonprehensile manipulation for rotating a deformable object using a plate with two degrees of freedom. Simulation model in (a) and the contact model in (b).

3. Manipulation Outline

In this section we give a brief explanation of the manipulation scheme and the simulation model used in this work, and then we show simulation and experimental results to validate the simulation model.

3.1. Manipulation Scheme

Figure 2 shows the manipulation of a deformable object on a plate in simulation. The plate has two degrees of freedom (DOF): the translational motion (DOF: X) and the rotational motion (DOF: Θ), along and around the horizontal axis, respectively. We give to the plate's two DOFs of motion sinusoidal trajectories:

$$\Theta(t) = -A_p \sin(2\pi f_p t) \quad \text{(1)}$$

$$X(t) = B_p \sin(2\pi f_p t) \quad \text{(2)}$$

where A_p, B_p, and f_p denote the angular amplitude, the linear amplitude, and the frequency of the plate motion, respectively. Under this plate motion, the object rotates with an angular velocity ω_B to the counter-clockwise direction when $A_p B_p < 0$, and to the clockwise direction when $A_p B_p > 0$ [11].

3.2. Simulation Model

For simulation analysis, we utilize the model, as shown in **Fig. 2(a)**, introduced in [13] to represent the dynamic behavior of a deformable object. This model is composed of virtual tile links, where each virtual tile has a node with mass m located at its center. Adjacent nodes are connected to each other by what we call a viscoelastic joint unit, which is composed by three DOFs: bending, compression/tension, and torsion. The bending and the compression joints have viscoelastic elements and the torsion joint is free. The simulation model in **Fig. 2(a)** is based on a circular slice of cheese with a diameter of 80 mm, with a mass of 13.6 g and negligible thickness, as shown in **Fig. 1(a)**. The object's model is composed of 52 virtual tile links of length 10 mm and 88 viscoelastic joint units, to approximate the real object. In this model, the friction coefficient between the plate and the object is assumed to be uniform and follow Coulomb's law, given by μ_s and μ_k for static and dynamic coefficients, respectively. The contact model between the plate and the i-th virtual link is shown in **Fig. 2(b)**, where the contact force is computed with the penalty method [19]. The contact force f_i^{contact} applied to each node is given by

$$f_i^{\text{contact}} = k_{\text{contact}} a_i^{2.2} + c_{\text{contact}} \dot{a}_i \quad (a_i \geq 0) \quad . \quad (3)$$

where a_i is the distance between the surface of the plate and that of the virtual link, k_{contact} and c_{contact} are the elasticity and viscosity, respectively. Based on [19], the nonlinearity of the elasticity in contact is considered. The frictional force f_i^{friction} applied to the node is given by,

$$f_i^{\text{friction}} = \mu_* f_i^{\text{contact}}. \quad . \quad . \quad . \quad . \quad . \quad . \quad . \quad . \quad . \quad . \quad . \quad (4)$$

where the coefficient of friction μ_* is defined by

$$\mu_* = \begin{cases} 0 & \text{for} \quad v_i^{\text{slip}} = 0 \\ \mu_s & \text{for} \quad 0 < |v_i^{\text{slip}}| < V \\ \mu_k & \text{for} \quad V \leq |v_i^{\text{slip}}| \end{cases}$$

where v_i^{slip} is the slip velocity of the i-th node with respect to the plate and V is the friction transition velocity, that determines the threshold between static and dynamic frictions. The frictional force f_i^{friction} is in the opposite direction to the slip velocity of the node with respect to the plate's surface. For all the simulations $V = 100$ mm/s, $k_{\text{contact}} = 11.86$ N/mm and $c_{\text{contact}} = 7.65 \times 10^{-3}$ are given empirically.

Figure 3 shows the behavior of a deformable object of $\omega_n = 10\pi$ rad/s for $A_p = 12$ deg, $B_p = 3$ mm, $f_p = 12$ Hz and a friction angle $\alpha = 36.9$ deg, this deformable object's bending parameters and friction angle were obtained from a slice of cheese, as reported in [13]. Here ω_n represents the first order natural angular frequency in bending, as shown in **Fig. 1(b)**, that is the frequency with which the object bends up and down freely, without any external forces nor restraints. This parameter depends on the mass of the nodes and the elasticity of the joint units of the model used for simulation. The friction angle between the plate and the object is defined as $\alpha = \tan^{-1}(\mu_s)$. Also,

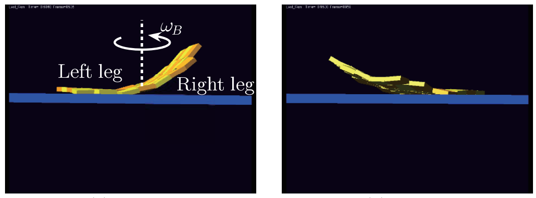

(a) $t = 0.58$ (b) $t = 0.95$

Fig. 3. Snapshots of the simulation for $f_p = 12$ Hz, $A_p = 12°$, $\omega_n = 10\pi$ rad/s and $\alpha = 36.9°$. The object is rotating on the plate with an angular velocity of $\omega_B = 344°$/s, by using a bipedal-gaited motion.

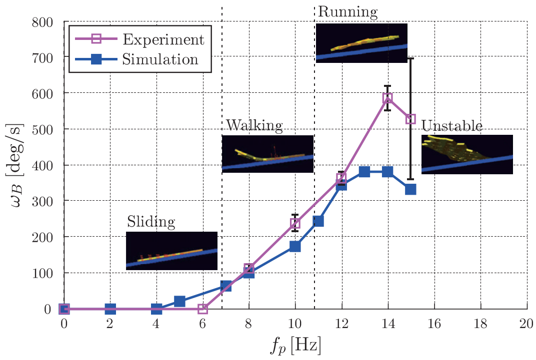

Fig. 4. Simulation and experimental results. The object's behavior changes similar to sliding, walking and running gaits [17].

we define $\mu_k = \beta \mu_s$, where $\beta = 0.53$ is empirically given. Therefore, when α changes it means that μ_s and μ_k also change. In **Fig. 3**, the object is rotating with an angular velocity of $\omega_B = 344°$/s.

Figure 4 shows the simulation and experimental results of a slice of cheese for $A_p = 12$ deg and $B_p = 3$ mm. It can be seen that in both experiment and simulation the maximal angular velocity of the object is achieved around the same angular frequency of the plate motion. If the object is divided into two parts by the line that passes through its center, and each half is regarded as left leg and right leg, the rotational motion of the object suggests a bipedal gait-like behavior on the floor [13], as illustrated in **Fig. 4**.

4. Object's Angular Velocity Characterization

In this section, based on simulation analysis we show how the curve representing the relationship between the object's angular velocity ω_B and the plate's frequency f_p can be described by a peak function such as the Lorentz one, and its similarity with the resonance phenomenon.

4.1. Object's Angular Velocity Transition

Let us now focus on the transition of the object's angular velocity ω_B, through simulation analysis. **Fig. 5(a)** shows examples of the relationship among the object's angular velocity ω_B, the plate's motion frequency f_p, and the plate's angular amplitude A_p for a deformable object of circular shape, with $\omega_n = 10\pi$ rad/s, a friction angle between the plate and the object of $\alpha = 36.9°$, and a trans-

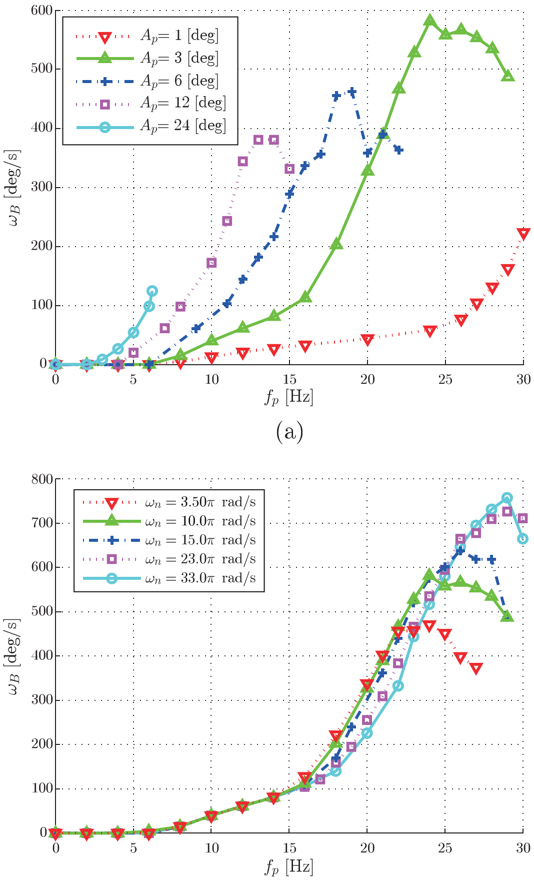

Fig. 5. Relationship between the object's angular velocity ω_B and the plate's motion frequency f_p with respect to (a) the plate's angular amplitude A_p for $\omega_n = 10\pi$ rad/s, and (b) the object's first order natural frequency in bending ω_n for $A_p = 3°$. Both (a) and (b) with $B_p = 3$ mm and $\alpha = 36.9°$.

lational amplitude $B_p = 3$ mm. From **Fig. 5(a)** we can obtain the optimum combination of f_p and A_p that generates the maximal angular velocity of the object. In this case, it can be seen that for $A_p = 3°$ the object has its maximal angular velocity $\omega_{B\max}$ around $f_p = 24$ Hz, and that for frequencies larger than this the object's angular velocity decreases as the object becomes unstable. We consider the object's behavior as unstable when the object is overturned or its center slips more than 10 mm from the center. The combination of f_p and A_p will determined when the object becomes unstable and these cases are not plot on **Fig. 5**. For this reason, in the extreme case of A_p being too large (24°) the plotted lines do not have a peak as in the other cases ($A_p = 3°$, 6°, and 12°). On the other hand, a plate amplitude of $A_p = 1°$ needs much larger frequencies of f_p for a peak to appear. **Fig. 5(b)** shows the relationship between f_p and ω_B for various deformable objects with different ω_n. From this figure, it can be seen that the frequency at which $\omega_{B\max}$ occurs, is uniquely determined for each of these deformable objects. Based on this observation, we can expect that the object's angular velocity transition mainly depends on ω_n.

In order to simplify the simulation analysis, in the following sections we suppose that all the deformable objects have the same negligible thickness, the same circular shape, and the same diameter of 80 mm. Also we only use $A_p = 3°$, 12°, and $B_p = 3$ mm for the plate's motion amplitudes.

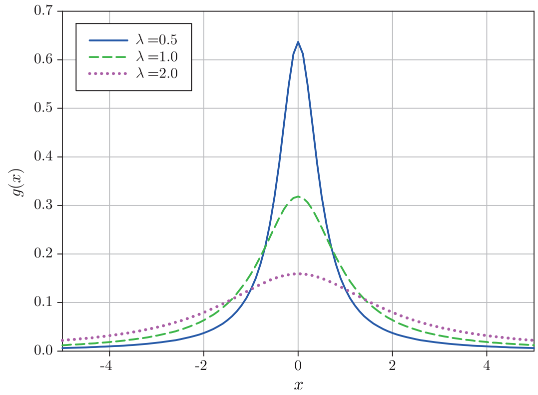

Fig. 6. Lorentz distribution for three different values of λ and $x_0 = 0$.

4.2. Resonance-Like Curve Fitting

The object's behavior suggests a peak line shape which is characteristic of a resonant behavior, i.e., the object's ω_B reaches its maximal amplitude $\omega_{B\max}$ only at the frequency of resonance. Taking advantage of this similarity, we employ a nonlinear regression analysis to represent the transition of the angular velocity of the object by a simple mathematical expression.

One of the most common functions describing a resonant behavior in curve fitting is the Lorentz distribution (also known as Cauchy distribution [20]) function:

$$g(x) = \frac{1}{\pi\lambda\left(1+\left(\dfrac{x-x_0}{\lambda}\right)^2\right)} \quad \ldots\ldots \quad (5)$$

where x_0 is the median of the distribution, λ is the half width at half maximal (HWHM) of the probability density function $g(x)$. These two parameters determine the shape of $g(x)$, and its maximal amplitude at $x = x_0$ is given by

$$a = \frac{1}{\pi\lambda}, \quad \ldots\ldots\ldots\ldots\ldots \quad (6)$$

which depends on the value of λ. **Fig. 6** shows the plot of Eq. (5) for three different values of λ and $x_0 = 0$. In this figure it can be seen that as the value of λ increases the value of the maximal amplitude of $g(x)$ decreases, as stated in Eq. (6). In order to have the maximal amplitude independent of the width of the curve, we now introduce a third parameter γ so that the maximal amplitude is given by

$$\tilde{a} = \frac{\gamma}{\pi\lambda}. \quad \ldots\ldots\ldots\ldots\ldots \quad (7)$$

Consequently, Eq. (5) is replaced by

$$\tilde{g}(x) = \frac{\tilde{a}}{1+\left(\dfrac{x-x_0}{\lambda}\right)^2}. \quad \ldots\ldots\ldots \quad (8)$$

In Eq. (7), the parameter γ can change the maximal amplitude, therefore we can have curves with the same maximal amplitude but different widths, that cannot be obtained by using Eq. (6). This third parameter γ allows the nonlinear regression to get a better approximation of the data to be fitted. Using Eq. (8) to express the transition of the object's angular velocity ω_B as a function of the plate's frequency f_p, we have

$$\omega_B(f_p) = \frac{\omega_{Br\max}}{1 + \left(\dfrac{f_p - f_0}{b}\right)^2}. \quad \text{. . . . . (9)}$$

where $\omega_{Br\max}$ is the maximal amplitude of ω_B at $f_p = f_0$, b is the HWHM and f_0 is the frequency at which $\omega_{Br} = \omega_{Br\max}$. The data analysis software Sigmaplot (Systat Software, Inc.) is utilized for the nonlinear regression analysis. This software uses the Marquardt-Levenberg algorithm to find the parameters $\omega_{Br\max}$, f_0, and b, that together with Eq. (9), yields the best approximation to the given data.

We carry out the nonlinear regression analysis of **Fig. 5(b)** for $\omega_n = 10\pi$ rad/s and $\omega_n = 33\pi$ rad/s with $\alpha = 36.9°$ by using Eq. (9), the resulting line shape is shown in **Figs. 7(a)** and **(b)**, respectively, where the dot line represents the simulation data and the solid line represents the regression line. The parameters obtained from this regression are $\omega_{Br\max} = 598.7°$/s, $b = 5.1$ Hz, and $f_0 = 25.1$ Hz, for $\omega_n = 10\pi$ rad/s and $\omega_{Br\max} = 746.9°$/s, $b = 5.8$ Hz, and $f_0 = 28.2$ Hz, for $\omega_n = 33\pi$ rad/s. Here the parameter f_0 can be regarded as a kind of frequency of resonance at which $\omega_{Br\max}$ occurs, and it can be seen that it is different for each object, as ω_n is different. The coefficient of determination is $R^2 = 0.99$ for $\omega_n = 10\pi$ rad/s and $R^2 = 0.99$ for $\omega_n = 33\pi$ rad/s are obtained. Additionally, the nonlinear regression analysis for $\omega_n = 10\pi$ rad/s and $\alpha = 56.3$ deg, is shown in **Fig. 7(c)**. The parameters obtained from this regression are $\omega_{Br\max} = 520.9°$/s, $b = 5.8$ Hz, $f_0 = 24.6$ Hz, and $R^2 = 0.98$. If we compare the result in **Fig. 7(c)** with the one from **Fig. 7(a)**, it can be observed that their f_0 are almost the same, while the values of $\omega_{Br\max}$ and b are different. The results in **Fig. 7** imply that two physical parameters ω_n and α determine the combinations of the regression parameters $\omega_{Br\max}$, f_0, and b.

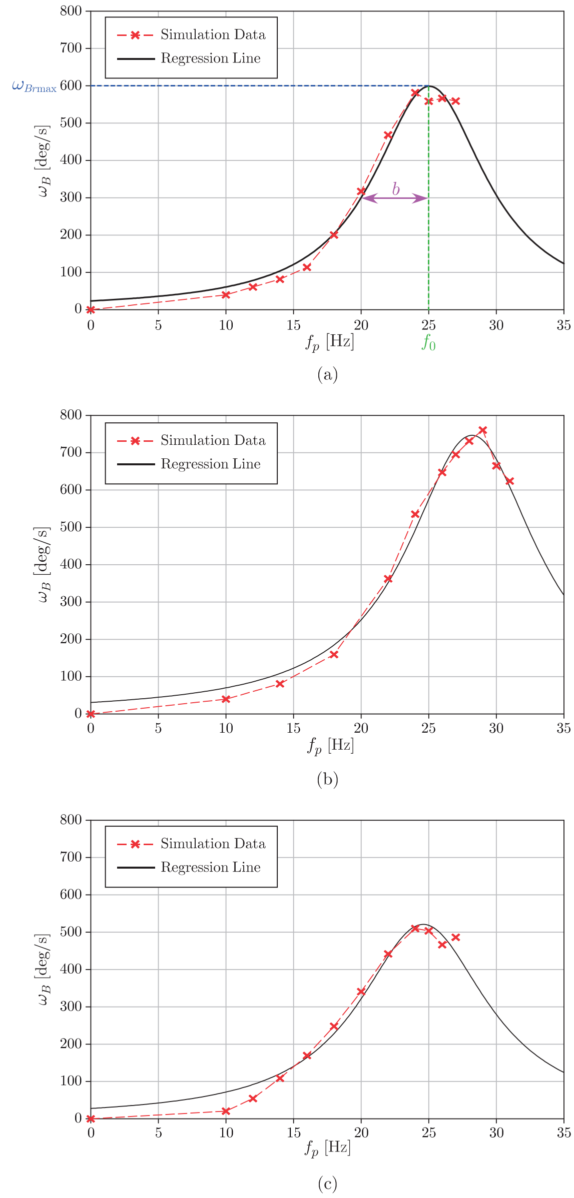

Fig. 7. Relationship between the object's angular velocity ω_B and the plate's frequency f_p, for (a) $\omega_n = 10\pi$ rad/s, $\alpha = 36.9°$, (b) $\omega_n = 33\pi$ rad/s, $\alpha = 36.9°$, and (c) $\omega_n = 10\pi$ rad/s, $\alpha = 56.3°$.

5. Inverse Problem: Object's Physical Parameter Identification

In this section, based on the curve fitting of the object's angular velocity ω_B line shape, we propose an identification method of the object's natural bending frequency ω_n that is supposed to mainly dominate the object's angular velocity line shape as mentioned in Section 4.

Figure 8 shows the relationship between the object's angular velocity ω_B and the plate's motion frequency f_p, for different friction angles α and different deformable objects, that is ω_n is different, for plate amplitudes of $A_p = 3°$ in **(a)** and $A_p = 12°$ in **(b)**. **Fig. 9** shows the values of $\omega_{Br\max}$ resulting from the nonlinear regression analysis of the simulation data of **Fig. 8**, where $A_p = 3°$ and $A_p = 12°$ are used in **Figs. 9(a)** and **(b)**, respectively. From this figure it can be seen that the value of $\omega_{Br\max}$ increases as ω_n increases. The thick straight line represents the regression line between $\omega_{Br\max}$ and ω_n that has a coefficient of determination of $R^2 = 0.93$ and 0.83, for $A_p = 3°$ and 12°, respectively. However, it can be observed that for each ω_n the value of $\omega_{Br\max}$ also changes depending on the friction angle α, particularly for the biggest two α in **Fig. 9(a)**. And, it can be observed that for each ω_n the value of $\omega_{Br\max}$ changes significantly depending on the friction angle α in particular for the two deformable objects with higher ω_n in **Fig. 9(b)**. From this relationship it is difficult to decompose the effects of ω_n and α on

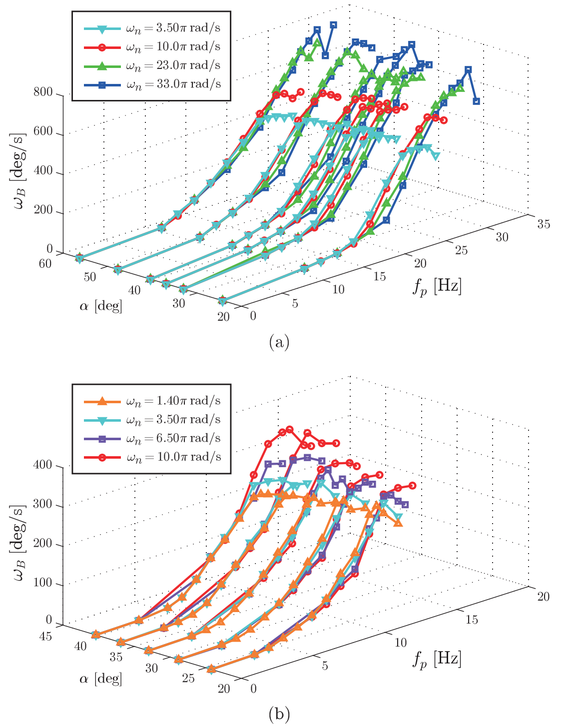

Fig. 8. Relationship between the object's angular velocity ω_B and the plate's motion frequency f_p, for different friction angles α and different deformable objects for (a) $A_p = 3°$ and (b) $A_p = 12°$, with $B_p = 3$ mm.

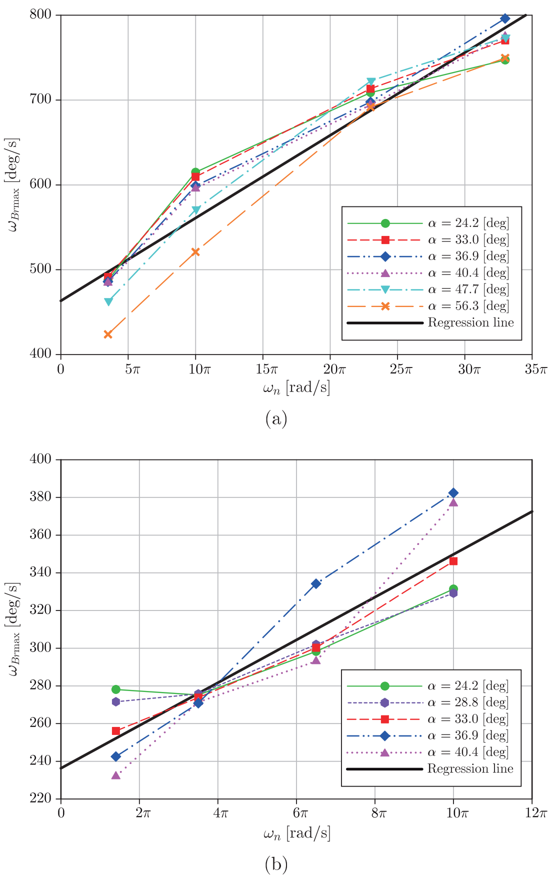

Fig. 9. Relationship between the object's first order natural angular frequency in bending ω_n and the parameter $\omega_{Br\max}$ obtained from the nonlinear regression of f_p vs. ω_B, for (a) $A_p = 3°$ and (b) $A_p = 12°$, with $B_p = 3$ mm.

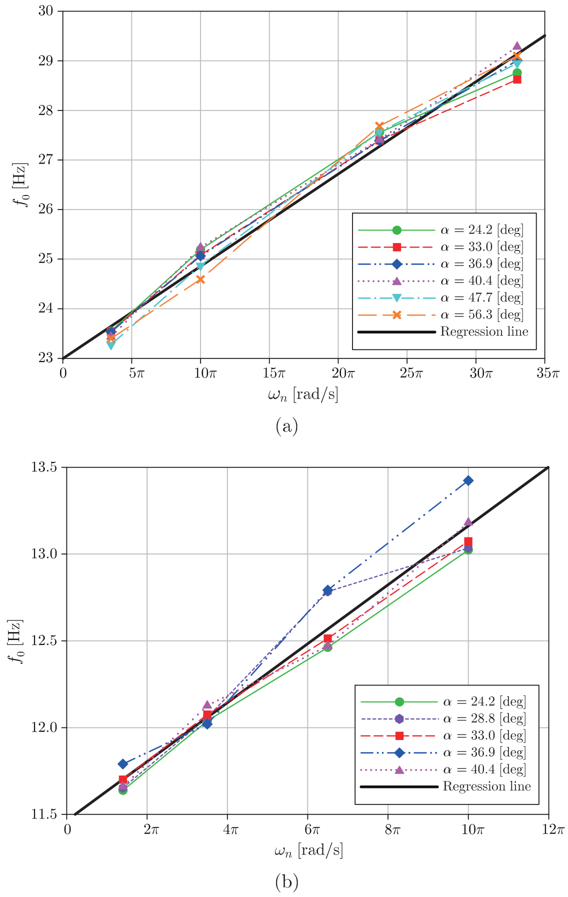

Fig. 10. Relationship between the object's first order natural angular frequency in bending ω_n and the parameter f_0 obtained from the nonlinear regression of f_p vs. ω_B, for (a) $A_p = 3°$ and (b) $A_p = 12°$, with $B_p = 3$ mm.

$\omega_{Br\max}$. This means that ω_n cannot be estimated simply by observing $\omega_{Br\max}$.

We next focus on the parameter f_0. **Fig. 10(a)** shows the results of the parameter f_0 with respect to ω_n for $A_p = 3°$ and the same friction angles in **Fig. 8(a)**. In the same way, **Fig. 10(b)** shows the results of f_0 with respect to ω_n for $A_p = 12°$. In **Fig. 10**, it can be seen that the value of f_0 increases as ω_n increases for each α, and that the value of f_0 does not change significantly for the same ω_n and different α. Here, the thick straight line represents the regression line between f_0 and ω_n that has a coefficient of determination of $R^2 = 0.99$ for $A_p = 3°$ in **Fig. 10(a)** and $R^2 = 0.96$ for $A_p = 12°$ in **Fig. 10(b)**, which are better than those obtained in **Figs. 9(a)** and **(b)**, respectively. The lines for almost all the different α have a similar slope with the regression line. This result suggests that the object's ω_n can be estimated by a linear equation as a function of f_0, regardless of the friction angle α, as follows,

$$\hat{\omega}_n = p_1 f_0 + q_1 \quad \ldots\ldots\ldots\ldots (10)$$

for each of the plate amplitudes A_p. Therefore, if we obtain f_0 from the curve fitting of the relationship between the object's angular velocity ω_B and the plate's frequency f_p, then we can estimate the value of the object's natural angular frequency in bending ω_n.

The frequency f_0 when $A_p = 3°$ is in the range of $23 <$

$f_0 < 30$ Hz, as shown in **Fig. 10(a)**, while the frequency f_0 when $A_p = 12°$ is in the range of $11 < f_0 < 14$ Hz, as shown in **Fig. 10(b)**. Therefore, $A_p = 12°$ is convenient from the experimental point of view of the actuators. However, for a plate amplitude of $A_p = 12°$ the object easily becomes unstable or folded in half. As a result, it can only deal with objects whose ω_n are less than 12π rad/s.

6. Validation of the Proposed Method

In this section we show the simulation and experimental results and the regression analysis of the real parameters against the estimated ones to confirm the validity of the proposed method.

6.1. Simulation Results

Using the data of **Fig. 10**, the parameters obtained from the linear regression are $p_1 = 5.30$, $q_1 = -121.62$ for $A_p = 3°$, and $p_1 = 5.65$, $q_1 = -64.51$ for $A_p = 12°$ in Eq. (10). Using these parameters in Eq. (10), we estimate the object's natural bending frequency.

The results are shown in **Fig. 11** for $A_p = 3°$ in **(a)** and $A_p = 12°$ in **(b)**. In this figure, ω_n denotes the object's natural bending frequency given to the simulation model and $\hat{\omega}_n$ denotes the estimated one using Eq. (10). The solid line is the result of the linear regression of the real data and the estimated one. In **Fig. 11(a)**, it can be seen, the estimated values are close to the real ones, the coefficient of determination is $R^2 = 0.99$. The regression line should ideally have a unit slope and an intercept of zero, that is, the estimated value is identical to the real one. In this case, it has a slope of 0.99 and an intercept of 0.25, which are close enough to their ideal values. Similarly, in **Fig. 11(b)** the coefficient of determination is $R^2 = 0.96$ for $A_p = 12°$. In this case, the regression line has a slope of 0.96 and an intercept of 0.24, which are also close enough to their ideal values.

6.2. Experimental Results

For validating the proposed method we carried out experiments with a real slice of cheese, the skin of a Chinese dumpling and a real slice of cheese with lead balls used in order to increase its weight. The three objects have the same circular shape with a radius of 40 mm, and the masses of the cheese, skin of Chinese dumpling and cheese with lead balls are 13.6 g, 6.9 g, and 39.5 g, respectively. **Fig. 12** shows the experimental results of the relationship between the object's angular velocity ω_B and the plate's frequency f_p, for the three deformable objects described above, when the plate motion is given by $A_p = 12°$ and $B_p = 3$ mm. The solid line represents the regression line for Eq. (9). From **Fig. 12** it can be seen that the experimental values can be described by its corresponding regression line, since $R^2 = 0.98$ for the slice of cheese, $R^2 = 0.98$ for the skin of a Chinese dumpling and $R^2 = 0.99$ for the slice of cheese with lead balls, were obtained.

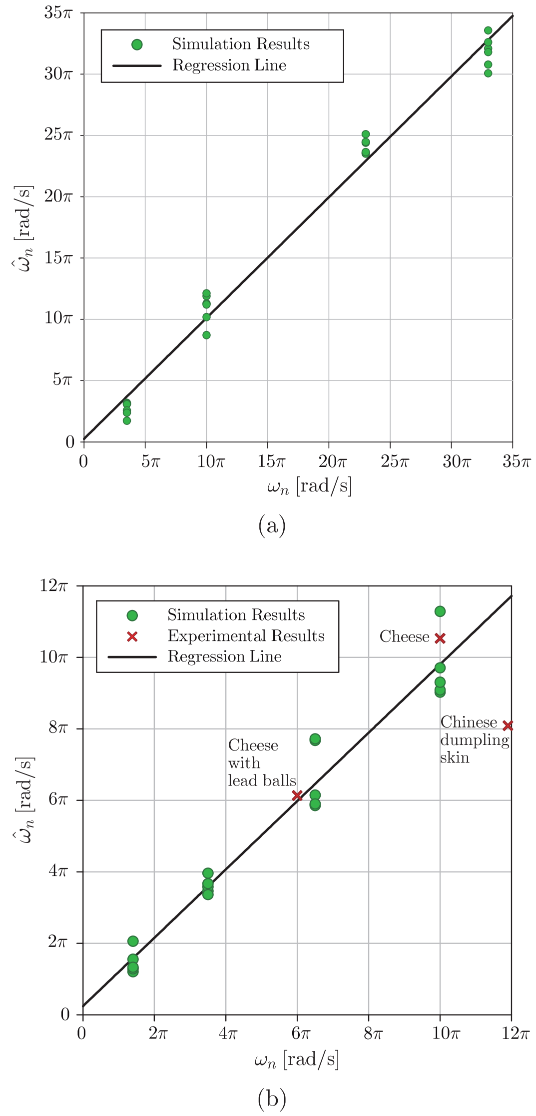

Fig. 11. Linear regression between the object's real ω_n (first natural angular frequency in bending) and the estimated $\hat{\omega}_n$ obtained by using Eq. (10). Simulation results for $A_p = 3°$ in (a) and simulation and experimental results for $A_p = 12°$ in (b).

The real ω_n and the estimated $\hat{\omega}_n$ values of the experimental data are overlapped on the simulation data, as shown in **Fig. 11(b)**. In the experimental results, as a real value of ω_n, we employ the cantilever based method used in [13] utilizing a piece of cut food and a high speed vision system of 400 fps to measure this parameter. The estimated parameter $\hat{\omega}_n$ is the one obtained from using Eq. (10) in the same way as with the simulation data.

In this case, the slice of cheese and the skin of the Chinese dumpling have similar natural bending frequencies. However, the skin of the Chinese dumpling is lighter than the slice of cheese, which suggests that the skin of the Chinese dumpling has a bending stiffness smaller than the one of the cheese. In contrast, the slice of cheese with lead balls, has a smaller bending frequency than the one for the slice of cheese only. This was expected as the lead balls increased the weight of the cheese, thus altering its mass-elasticity ratio.

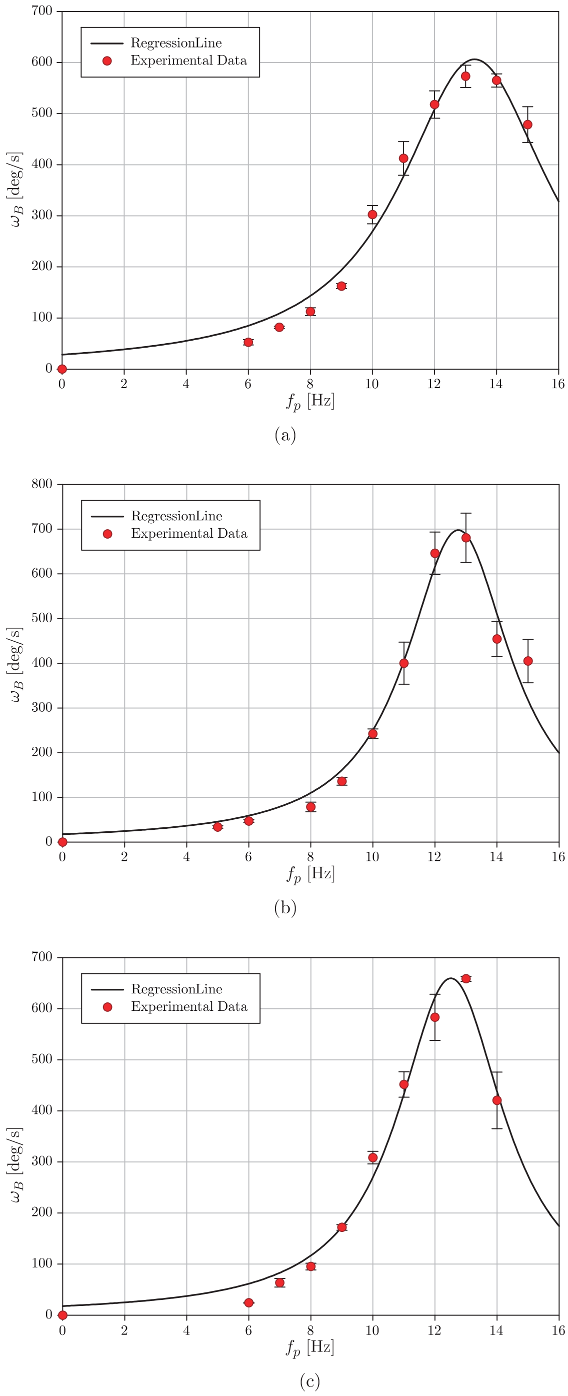

Fig. 12. Relationship between the object's angular velocity ω_B and the plate's frequency f_p, for (a) a slice of cheese, (b) the skin of a Chinese dumpling and (c) a slice of cheese with lead balls, with $A_p = 12°$ and $B_p = 3$ mm.

6.3. Discussion

As mentioned earlier in Section 1, a high frequency of the object's bending vibration is converted to a rotating motion of low frequency. The object's frequency of rotation f_B on the plate can be obtained from the object's maximal angular velocity $\omega_{Br\max}$ in **Fig. 9**, for each of the four deformable objects and each of the two plate amplitudes A_p used in this paper. The results of f_B are shown in **Table 1**, where the object's bending vibration frequency f_n is

Table 1. Object's first order natural frequency in bending and its frequency of rotation.

A_p [deg]	ω_n [π rad/s]	f_n [Hz]	$\omega_{Br\max}$ [deg/s]	f_B [Hz]
3	3.50	1.75	491.5	1.36
	10.0	5.00	614.9	1.71
	23.0	11.5	722.8	2.01
	33.0	16.5	796.1	2.21
12	1.40	0.70	278.1	0.77
	3.50	1.75	275.8	0.77
	6.50	3.25	334.2	0.93
	10.0	5.00	382.4	1.06

also shown. It should be noted that especially for the deformable object of $\omega_n = 33\pi$ rad/s, its bending vibration frequency of $f_n = 16.5$ Hz is converted into a rotational motion with a frequency of $f_B = 2.21$ Hz, for $A_p = 3°$. This represents only the 13.4% of the object's bending frequency f_n. Thus, the object's first order natural angular frequency in bending ω_n can be measured through the object's dynamic behavior, observing its low frequency rotation motion f_B and Eq. (10), by using the manipulation scheme presented in this work.

7. Conclusion

This paper discussed the characterization of a thin deformable object by using dynamic nonprehensile manipulation. We showed that the line shape of the angular velocity of the object with respect to the plate's frequency has a resonance-like behavior. Based on this nature, we showed that the object's angular velocity transition can be represented with a simple mathematical expression like the Lorentz distribution one, instead of a complex expression derived from the dynamics of the system. We found out that the frequency of resonance at which the object's maximal angular velocity occurs, depends on the first order natural angular frequency in bending of the object. As an inverse problem, we proposed how to identify the above physical parameter of the object from the regression parameters in the Lorentzian curve fitting. We verified the proposed method by using simulation data and experimental data.

In the future, we would like to investigate the influence of the object's shape, thickness, and the friction between the object and the plate, and analyze the role of the viscosity and water components in the object's resonance-like behavior. Then, it may be possible to evaluate the mass, elasticity, viscosity and friction of the deformable object by characterizing its rotational behavior on a simple flat plate considering not only the object's first order frequency of vibration but also higher orders.

References:

[1] K. M. Lynch and M. T. Mason, "Dynamic nonprehensile manipulation: controllability, planning, and experiments," Int. J. Robot. Res., Vol.18, No.8, pp. 64-92, 1999.

[2] A. Amagai and K. Takase, "Implementation of dynamic manipulation with visual feedback and its application to pick and place task," in Proc. IEEE Int. Symp. Assem. Task Planning, pp. 344-350, 2001.

[3] D. Reznik, E. Moshkovich, and J. Canny, "Building a universal planar manipulator," in Proc. Workshop Dist. Manip. at Int. Conf. Robot. Autom., 1999.

[4] D. Reznik and J. Canny, "C'mon part, do the local motion!," in Proc. IEEE Int. Conf. Robot. Autom., pp. 2235-2242, 2001.

[5] K. F. Böhringer, B. Donald, and N. MacDonald, "Sensorless manipulation using massively parallel microfabricated actuator arrays," in Proc. IEEE Int. Conf. Robot. Autom., Vol.1, pp. 826-833, 1994.

[6] K. F. Böhringer, V. Bhatt, and K. Goldberg, "Sensorless manipulation using transverse vibrations of a plate," in Proc. IEEE Int. Conf. Robot. Autom., pp. 1989-1986, 1995.

[7] K. F. Böhringer, K. Goldberg, M. Cohn, R. Howe, and A. Pisano, "Parallel microassembly with electrostatic force fields," in Proc. IEEE Int. Conf. Robot. Autom., Vol.2, pp. 1204-1211, 1998.

[8] T. Vose, P. Umbanhowar, and K. M. Lynch, "Friction-induced velocity fields for point parts sliding on a rigid oscillated plate," Int. J. Robot. Res., Vol.28, No.8, pp. 1020-1039, Aug. 2009.

[9] T. Vose, P. Umbanhowar, and K. M. Lynch, "Friction-induced lines of attraction and repulsion for parts sliding on a oscillated plate," IEEE Trans. Autom. Sci. Eng., Vol.6, pp. 685-699, Oct. 2009.

[10] T. Vose, P. Umbanhowar, and K. M. Lynch, "Toward the set of frictional velocity fields generable by 6-degree-of-freedom oscillatory motion of a rigid plate," in Proc. IEEE Int. Conf. Robot. Autom., pp. 540-547, 2010.

[11] M. Higashimori, K. Utsumi, Y. Omoto, and M. Kaneko, "Dynamic manipulation inspired by the handling of a pizza peel," IEEE Trans. Robot., Vol.25, pp. 829-838, Aug. 2009.

[12] M. Higashimori, Y. Omoto, and M. Kaneko, "Non-grasp manipulation of deformable object by using pizza handling mechanism," in Proc. IEEE Int. Conf. Robot. Autom., Kobe, Japan, pp. 120-125, 2009.

[13] I. G. Ramirez-Alpizar, M. Higashimori, M. Kaneko, C.-H. D. Tsai, and I. Kao, "Dynamic nonprehensile manipulation for rotating a thin deformable object: an analogy to bipedal gaits," IEEE Trans. Robot., Vol.28, pp. 607-618, June 2012.

[14] I. G. Ramirez-Alpizar, M. Higashimori, and M. Kaneko, "Estimation of a thin flexible object with bipedal gaits," in Proc. IEEE Int. Conf. on Autom. Sci. and Eng., Seoul, Korea, pp. 952-957, 2012.

[15] S. Hirai, "Transferring human motion to mechanical manipulator in insertion of deformable tubes," J. of Robotics and Mechatronics, Vol.10, No.3, pp. 209-213, 1998.

[16] K. Salleh, H. Seki, Y. Kamiya, and M. Hikizu, "Tracing manipulation in clothes spreading by robot arms," J. of Robotics and Mechatronics, Vol.18, No.5, pp. 564-571, 2006.

[17] K. S. M. Sahari, H. Seki, Y. Kamiya, and M. Hikizu, "Passive edge tracing of deformable object by robot," J. of Robotics and Mechatronics, Vol.23, No.3, pp. 458-461, 2011.

[18] K. Koo, X. Jiang, A. Konno, and M. Uchiyama, "Development of a wire harness assembly motion planner for redundant multiple manipulators," J. of Robotics and Mechatronics, Vol.23, No.6, pp. 907-918, 2011.

[19] M. Moore and J. Wihelms, "Collision detection and response for computer animation," Comput. Graphics, Vol.22, No.4, pp. 289-298, 1988.

[20] J. K. Patel, C. H. Kapadia, and D. B. Owen, "Handbook of statistical distributions," Marcel Dekker, Inc., p. 212, 1976.

Name:
Ixchel G. Ramirez-Alpizar

Affiliation:
Ph.D. Student, Department of Mechanical Engineering, Graduate School of Engineering, Osaka University

Address:
2-1 Yamadaoka, Suita, Osaka 565-0871, Japan

Brief Biographical History:
2005- B.S. degree in Electronic Engineering from Universidad Autonoma Metropolitana
2010 M.E. degree in Electronic and Control Systems Engineering from Shimane University
2010- Ph.D. Student, Graduate School of Engineering, Osaka University

Main Works:
• I. G. Ramirez-Alpizar, M. Higashimori, M. Kaneko, C-H. D. Tsai, and I. Kao, "Dynamic Nonprehensile Manipulation for Rotating a Thin Deformable Object: an Analogy to Bipedal Gaits," IEEE Trans. on Robotics, Vol.28, No.3, pp. 607-618, Jun. 2012.

Membership in Academic Societies:
• The Institute of Electrical and Electronic Engineers (IEEE)
• The Japan Society of Mechanical Engineers (JSME)
• The Robotics Society of Japan (RSJ)

Name:
Mitsuru Higashimori

Affiliation:
Associate Professor, Department of Mechanical Engineering, Graduate School of Engineering, Osaka University

Address:
2-1 Yamadaoka, Suita, Osaka 565-0871, Japan

Brief Biographical History:
1998 M.E. degree in Information Engineering from Hiroshima University
1998- Toshiba Corporation
2002- Research Associate, Department of Artificial Complex Systems Engineering, Hiroshima University
2006 Ph.D. degree in Artificial Complex Systems Engineering from Hiroshima University
2006- Research Associate, Department of Mechanical Engineering, Osaka University
2008- Associate Professor, Department of Mechanical Engineering, Osaka University

Main Works:
• M. Higashimori, K. Utsumi, Y. Omoto, and M. Kaneko, "Dynamic Manipulation Inspired by the Handling of a Pizza Peel," IEEE Trans. on Robotics, Vol.25, No.4, pp. 829-838, 2009.
• M. Higashimori, M. Kimura, I. Ishii, and M. Kaneko, "Dynamic Capturing Strategy for a 2-D Stick-Shaped Object Based on Friction Independent Collision," IEEE Trans. on Robotics, Vol.23, No.3, pp. 541-552, 2007.

Membership in Academic Societies:
• The Society of Instrument and Control Engineers (SICE)
• The Robotics Society of Japan (RSJ)
• The Japan Society of Mechanical Engineers (JSME)
• The Institute of Electrical and Electronics Engineers (IEEE)

Name:
Makoto Kaneko

Affiliation:
Professor, Department of Mechanical Engineering, Graduate School of Engineering, Osaka University

Address:
2-1 Yamadaoka, Suita, Osaka 565-0871, Japan

Brief Biographical History:

1981 Ph.D. degree in Mechanical Engineering from The University of Tokyo

1981-1990 Researcher, Mechanical Engineering Laboratory (MEL), Ministry of International Trade and Industry (MITI)

1988-1989 Post-Doctoral Fellow, Technical University Darmstadt, Germany

1990-1993 Associate Professor, Computer Science and System Engineering, Kyushu Institute of Technology

1991-1992 Invited Professor, Technical University of Darmstadt, Germany

1993-2006 Professor, Industrial Engineering Department, Hiroshima University

2006- Professor, Department of Mechanical Engineering, Osaka University

Main Works:

• N. Tanaka, M. Higashimori, M. Kaneko, and I. Kao, "Noncontact Active Sensing for Viscoelastic Parameters of Tissue with Coupling Effect," IEEE Trans. on Biomedical Engineering, Vol.58, No.4, pp. 509-520, 2011.

• T. Kawahara, Y. Miyata, K. Akayama, M. Okajima, and M. Kaneko, "Design of Noncontact Tumor Imager for Video-Assisted Thoracic Surgery," IEEE Trans. on Mechatronics, Vol.15, No.6, pp. 838-846, 2010.

Membership in Academic Societies:

• The Institute of Electrical and Electronics Engineers (IEEE) Robotics and Automation Society

• The Institute of Electrical and Electronics Engineers (IEEE) Systems, Man, and Cybernetics Society

• The Institute of Electrical and Electronics Engineers (IEEE) Industrial Electronics Society

• The Japan Society of Mechanical Engineers (JSME)

• The Society of Instrument and Control Engineers (SICE)

• The Robotics Society of Japan (RSJ)